

## Initial mechanisms for the unimolecular decomposition of electronically excited nitrogen-rich energetic salts with tetrazole rings: $(\text{NH}_4)_2\text{BT}$ and TAGzT

Bing Yuan and Elliot R. Bernstein

Citation: *The Journal of Chemical Physics* **145**, 064306 (2016); doi: 10.1063/1.4960345

View online: <http://dx.doi.org/10.1063/1.4960345>

View Table of Contents: <http://aip.scitation.org/toc/jcp/145/6>

Published by the *American Institute of Physics*

---

### Articles you may be interested in

Initial mechanisms for the unimolecular decomposition of electronically excited nitrogen-rich energetic materials with tetrazole rings: 1-DTE, 5-DTE, BTA, and BTH

*The Journal of Chemical Physics* **144**, 234302 (2016); doi: 10.1063/1.4953552

---



**COMPLETELY  
REDESIGNED!**

*Physics Today* Buyer's Guide  
Search with a purpose.

# Initial mechanisms for the unimolecular decomposition of electronically excited nitrogen-rich energetic salts with tetrazole rings: $(\text{NH}_4)_2\text{BT}$ and TAGzT

Bing Yuan and Elliot R. Bernstein<sup>a)</sup>

*Department of Chemistry, Colorado State University, Fort Collins, Colorado 80523-1872, USA*

(Received 2 June 2016; accepted 22 July 2016; published online 10 August 2016)

Unimolecular decomposition of nitrogen-rich energetic salt molecules bis(ammonium)5,5'-bistetrazolate  $(\text{NH}_4)_2\text{BT}$  and bis(triaminoguanidinium) 5,5'-azotetrazolate TAGzT, has been explored via 283 nm laser excitation. The  $\text{N}_2$  molecule, with a cold rotational temperature ( $<30$  K), is observed as an initial decomposition product, subsequent to UV excitation. Initial decomposition mechanisms for the two electronically excited salt molecules are explored at the complete active space self-consistent field (CASSCF) level. Potential energy surface calculations at the CASSCF(12,8)/6-31G(d)  $(\text{NH}_4)_2\text{BT}$  and ONIOM (CASSCF/6-31G(d):UFF) (TAGzT) levels illustrate that conical intersections play an essential role in the decomposition mechanism as they provide non-adiabatic, ultrafast radiationless internal conversion between upper and lower electronic states. The tetrazole ring opens on the  $S_1$  excited state surface and, through conical intersections  $(S_1/S_0)_{\text{CI}}$ ,  $\text{N}_2$  product is formed on the ground state potential energy surface without rotational excitation. The tetrazole rings open at the  $\text{N}_2\text{—N}_3$  ring bond with the lowest energy barrier: the  $\text{C—N}$  ring bond opening has a higher energy barrier than that for any of the  $\text{N—N}$  ring bonds: this is consistent with findings for other nitrogen-rich neutral organic energetic materials. TAGzT can produce  $\text{N}_2$  either by the opening of tetrazole ring or from the  $\text{N=N}$  group linking its two tetrazole rings. Nonetheless, opening of a tetrazole ring has a much lower energy barrier. Vibrational temperatures of  $\text{N}_2$  products are hot based on theoretical predictions. Energy barriers for opening of the tetrazole ring for all the nitrogen-rich energetic materials studied thus far, including both neutral organic molecules and salts, are in the range from 0.31 to 2.71 eV. Energy of the final molecular structure of these systems with dissociated  $\text{N}_2$  product is in the range from  $-1.86$  to  $3.11$  eV. The main difference between energetic salts and neutral nitrogen-rich energetic material is that energetic salts usually have lower excitation energy. *Published by AIP Publishing.* [<http://dx.doi.org/10.1063/1.4960345>]

## I. INTRODUCTION

The initial decomposition reaction, activated by electronic excitation, for two nitrogen rich tetrazole based isolated, energetic salt molecules in the gas phase is studied both experimentally and theoretically. In this context, energetic salt molecules (species) are those that form a crystal of a condensed phase energetic salt material.<sup>1,2</sup>

Synthesis of new heterocyclic based energetic salts appeared a decade ago: these molecules are difficult to detect and their low vapor pressures essentially eliminated the risk of exposure through inhalation.<sup>3</sup> Their properties are optimized and improved through the combination of different cations and anions, as well as by independent modification of cationic and anionic components.<sup>3</sup> The most promising heterocyclic backbone for preparation of high-performance nitrogen-rich energetic material is considered to be the tetrazole ring.<sup>4</sup> The tetrazole ring is a five-membered aromatic heterocycle, containing four nitrogen atoms and one carbon atom, with a high heat of formation resulting from inherently energetic  $\text{N—N}$  and  $\text{C—N}$  bonds, high strain, and high density.<sup>4</sup> During

decomposition, the  $\text{N—N}$  and  $\text{C—N}$  bonds are converted to form  $\text{N}_2$ , an extremely stable and environmentally green molecule, with a large amount of energy being released from the molecular system.<sup>5</sup>

The corresponding nitrogen-rich salts of 5,5'-bistetrazoles have one of the highest nitrogen contents of any tetrazole ring derivative, and have been the focus of research and application as a low-smoke pyrotechnic fuel for decades.<sup>4</sup> In these salts, the observed  $\text{N—N}$  and  $\text{C—N}$  bond lengths both lie between typical values for single and double bonds and show good agreement with bond lengths in common aromatic heterocycles.<sup>6</sup> The torsion angles for the bistetrazole rings indicate a completely planar ring system for the whole anion, which together with the bond lengths lead to the assumption of a large  $6\pi$ -electron aromatic system.<sup>4</sup> Diammonium 5,5'-bistetrazolate  $(\text{NH}_4)_2\text{BT}$  is one of the tetrazole based energetic salts upon which we focus in this study: its isolated molecule structure is shown in Figure 1. The crystal structure of  $(\text{NH}_4)_2\text{BT}$  is a layered topology in which the bistetrazolate moieties are connected over the ammonium cations via a hydrogen-bonding network.<sup>4,6</sup> The nitrogen content of  $(\text{NH}_4)_2\text{BT}$  is 81.36 wt. % and its decomposition temperature is  $312^\circ\text{C}$ .<sup>4</sup>  $(\text{NH}_4)_2\text{BT}$  shows low sensitivities toward both impact (35 J) and friction ( $>360$  N).<sup>4</sup> The detonation velocity

<sup>a)</sup> Author to whom correspondence should be addressed. Electronic mail: [erb@Colostate.edu](mailto:erb@Colostate.edu)

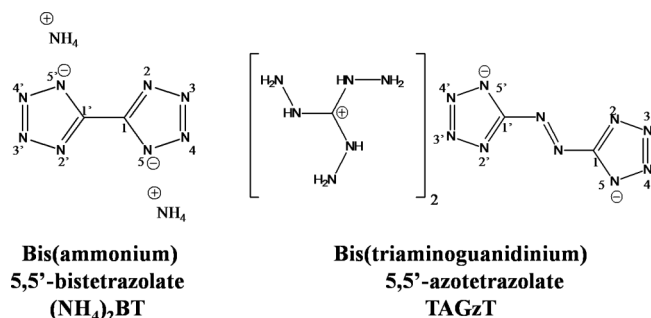


FIG. 1. Chemical structures of (NH<sub>4</sub>)<sub>2</sub>BT and TAGzT with atoms numbered for the rings.

of (NH<sub>4</sub>)<sub>2</sub>BT equals 7417 m/s, which is comparable to that for TNT.<sup>4</sup>

The azo-couplings of nitrogen-rich heterocycles, such as 5,5'-azotetrazolate dianion (zT<sup>2-</sup>) salts, are particularly interesting because of their high heat of formation, and high molar and volumetric gas production.<sup>2,7</sup> TAGzT, which consists of two triaminoguanidinium cations and one divalent azotetrazolate anion, is the other energetic salt studied in this work (molecular structure is shown in Figure 1) and it shows promise as a propellant additive because of its exceptionally high burning rate.<sup>5,8</sup> The carbon, nitrogen, and three amino hydrogen atoms in the triaminoguanidinium cation are nearly coplanar.<sup>5</sup> The azotetrazolate dianion consists of two identical coplanar, five-membered tetrazole rings, whose carbon atoms bond to each side of the N=N azo functional group. Two C—N bonds and three N—N bonds in each tetrazole ring all contain double-bond character as a result of  $\pi$ -electron delocalization.<sup>5</sup> The TAGzT material is a bright yellow, needle-like crystalline solid with a decomposition temperature of 209.2 °C and a nitrogen content of 82 wt. %.<sup>5,7</sup> The impact sensitivity and friction sensitivity of TAGzT are 4 J (RDX = 5 J) and 60 N (dry PETN = 60 N), respectively, which imply that TAGzT is a relatively sensitive energetic salt.<sup>9</sup> The detonation velocity of TAGzT is 7654 m/s, comparable to the value of TNT.<sup>9</sup> Based on previous studies, the major explosion product for TAGzT is N<sub>2</sub>,<sup>2,7,9</sup> which has been identified with mass spectrometry ( $m/z = 28$ ), as well as by its characteristic purple gas-phase discharge color using a high-frequency brush electrode.<sup>9</sup> Decomposition is initiated by the opening of tetrazole ring and the tetrazole ring decomposes to nitrilimines under release of nitrogen N<sub>2</sub> as the main decomposition step.<sup>1,2,9</sup> Near 195 °C, the triaminoguanidinium cation decomposes through the elimination of hydrazine, which subsequently decomposes to form HNCNH and NH<sub>3</sub> (or N<sub>2</sub>H<sub>4</sub>) as main products.<sup>1,9</sup>

We focus on the decomposition of isolated energetic salt molecules experimentally, and calculate the decomposition mechanism of single energetic salt species theoretically. Theoretical approaches are guided by the experimentally observed results for reactions, kinetics, and dynamics in order to generate the observations and to demonstrate that current, modern ideas of organic unimolecular decomposition processes are consistent with the ultrafast behavior of energetic molecular species and their properties. Two directions for explication of the release of stored energy from energetic

materials can be explored: study of the sensitivity, heat of formation, and denotation velocity in the solid state; and study of the initial bond dissociation reaction and decomposition mechanisms for the exothermic unimolecular chemical reactions driving detonation.<sup>10,11</sup> The latter approach, which we have pursued over the last decade,<sup>12–27</sup> emphasizes the isolated energetic molecule behavior as the essential first step in the energy release processes in either phase. In both gas phase and condensed phase, the first step of the decomposition mechanism is initiated by an endothermic chemical reaction, presumably the rupture of a local molecular bond.<sup>28,29</sup> In general, the difference between condensed phase and gas phase reactions is that solid state reactions occur within the rigid constraining environment of a crystal lattice, in which intermolecular interactions can influence reaction mechanisms and directions.<sup>30</sup> In the condensed phase in energetic salt material, intermolecular  $\pi$ -stacking and hydrogen-bonding interactions, which can affect the sensitivity and explosive behavior of energetic salts, are present.<sup>31,32</sup> The energy of these interactions is around 10–15 kcal/mol, much lower than the energy of chemical bond (>40 kcal/mol) in the isolated energetic salt molecules.<sup>33,34</sup> Although condensed phase reactions can be more complicated than gas phase ones, studies of the unimolecular behavior of explosives enable researchers to understand initial decomposition mechanisms and it represents a reasonable approximation to the primary initial behavior for their decomposition; moreover, they provide useful information toward the design of new energetic materials with low sensitivity and high denotation performance.<sup>10,28</sup>

Energetic materials are sensitive to stored energy release initiation by heat, electrostatic discharge, impact, friction, shock, and laser irradiation;<sup>33</sup> however, in which way the input energy can be concentrated to create sufficient energy localization to break an initial intramolecular bond to commence the exothermic decomposition reaction is still a very complicated problem.<sup>33</sup> Mechanisms have been proposed involving shock waves passing through an energetic solid that result in considerable intramolecular vibrational excitation, which leads to bond rupture in a high energy molecule: this is referred to as a multiphonon-vibron up-pumping mechanism.<sup>33,35</sup> In our studies, we have followed decomposition mechanisms starting from excited molecular electronic states. Based on the phenomenon of triboluminescence, it can be concluded that molecular electronic excitation must contribute to the initial chemical reactions that begin the release of stored molecular energy for an energetic system.<sup>36–42</sup> Consequently, our studies focus on the unimolecular decomposition mechanisms for electronically excited molecules comprising energetic materials. Both experiments and theory are explored in order to explicate the kinetics of and mechanisms for these initial processes.

When the excited states are involved, conical intersections, which are the potential crossing and non-adiabatic interaction points between two adiabatic electronic state surfaces, play a key role in the ultrafast (<100 fs) decomposition mechanisms, which successfully explain experimental observations.<sup>12–15,43–46</sup> The presented discussion includes product energy distribution, at the initial ultrafast

molecular level, following electronic excitation for the isolated energetic salts of interest. Although completely ground state processes can occur for these systems, they are in most instances not the main reaction paths for generation of observed products under the current experimental conditions.

In sum, in this work, energy resolved spectra of product molecule  $N_2$  are studied to define initial decomposition dynamics of the isolated energetic salt molecules  $(NH_4)_2BT$  and TAGzT: these spectra reflect the rotational temperature of the  $N_2$  product. Potential energy surfaces for the excited and ground electronic states of the two energetic salts  $(NH_4)_2BT$  and TAGzT are explored theoretically employing quantum chemistry calculations (Gaussian 09, CASSCF). The detailed decomposition mechanisms are thereby determined and discussed. As none of these energetic species contains an  $NO_2$  or an  $N_2O_2$  group, tetrazole ring opening decomposition mechanisms are calculated and proposed. These studies are both fundamental and practical as they make advances toward the application of fundamental chemical physics specifically to the behavior of new energy storage salt materials.

## II. EXPERIMENTAL PROCEDURES

The experimental setup consists of a matrix-assisted laser desorption (MALD) system, a supersonic jet expansion nozzle, and a time of flight mass spectrometer. Details of the instrumental design are described in our previous papers.<sup>13,14</sup> The nozzle used for the molecular beam generation is constructed from a Jordan Co. pulsed valve and a laser ablation attachment. The laser desorption head is attached to the front of the pulsed valve with three significant parts: (1) a  $2 \times 60$  mm channel for the expansion gas from the nozzle, (2) a conical channel (3 mm at the outside and 1 mm at the intersection with gas expansion channel) for the ablation laser beam perpendicular to the expansion gas channel, and (3) a 40 mm diameter hole for the sample drum. The sample drum fits into the 40 mm hole and is simultaneously rotated and translated by a motor and gear system in the vacuum in order to present a fresh sample region to the ablation laser for each pulse. The nonvolatile samples are desorbed from the drum by 532 nm ablation laser, entrained in the flow of He carrier gas under a pressure of 80 psi through the  $2 \times 60$  mm channel in the laser desorption head, and expanded into the vacuum chamber. With 80 psi He backing pressure for the closed pulsed valve, the chamber pressure remains at  $8 \times 10^{-8}$  Torr; with the valve open at 10 Hz, the chamber pressure increases to  $4 \times 10^{-7}$  Torr.

All sample drums for MALD are prepared by wrapping a piece of porous filter paper around a clean Al drum. A solution of 0.02 mol/l matrix (rhodamine 6G) and 0.01 mol/l  $(NH_4)_2BT$  or TAGzT in water is uniformly sprayed on the drum surface while it is rotating under a halogen heat lamp in a fume hood to make sure the sample coating is dry. Rhodamine 6G is chosen because it has an intense absorption at 532 nm; consequently, it can efficiently absorb the 532 nm laser photons, and decompose. This process expels the intact energetic molecules, trapped in the dye matrix, into the supersonic expansion gas flow from the pulsed nozzle.

An air atomizing spray nozzle (Spraying System Co.) with siphon pressure of 10 psi is used to deposit the energetic salt plus matrix on the filter paper surface. The dried drum with the well-distributed sample is then placed in the laser ablation head assembly and put into the vacuum chamber for decomposition reaction studies. Both energetic salts are supplied by Prof. Thomas M. Klapökte, Ludwig-Maximilian University of Munich.

Laser ablation process will generate both ionic and neutral species. In our apparatus, only the neutrals can enter the electric field extraction/ionization region because the plates are continuously charged to 4.00 kV and 3.75 kV, as is usual for a linear 1 m time of flight mass spectrometer with a 3 plate ion focusing region for laser ionization of neutrals. Negative ions entering this region are attracted to the high voltage plate and are not deflected toward the flight tube/detector, and positive ions undergo a curved deflection as they enter the high voltage field region and do not reach the microchannel detector at all or are dispersed by the field to generate only a background signal, which is known to be quite small ( $<1$  mV) by measurement.

In addition to the ablation laser, another laser is used to photo-excite the energetic sample in the beam and then detect the dissociated fragments. A single pump/probe laser is used at 283 nm for sample initiation and  $N_2$  detection following a one color ( $2 + 2$ ) resonance-enhanced four photon ionization (REMPI) scheme [ $a^1\Pi_g(v' = 1) \leftarrow X^1\Sigma_g(v'' = 0)$  and  $I \leftarrow a$  transitions] through time of flight mass spectrometry (TOFMS).<sup>47–49</sup> Note that the energetic salt sample is in a condensed phase ( $(NH_4)_2BT$  and TAGzT trapped in an R6G matrix) under 532 nm laser ablation, while for the 283 nm excitation/decomposition processes, it is in the form of an isolated energetic molecule. The UV laser wavelengths for this process are generated by a dye laser, pumped by the second harmonic (532 nm) of a Nd: yttrium aluminum garnet laser's fundamental output (1.064  $\mu\text{m}$ ), in conjunction with a frequency doubling system. As totally five or six photons are required in one decomposition and detection process (i.e.,  $(NH_4)_2BT$  can dissociate upon two photons absorption, TAGzT can dissociate upon one or two photon absorption), the typical pulse energy of the UV laser is ca. 5 mJ/pulse, giving an intensity of  $\sim 2 \times 10^9$  W/cm<sup>2</sup> for an 8 ns pulse duration at the sample. The molecular beam is perpendicularly crossed by the UV laser beam, which is focused to a spot size of about 0.2 mm diameter at the ionization region of the TOFMS. Before the detection of energetic salts, a 3%  $N_2$  in He gas mixture is prepared and studied for calibration of the  $N_2$  rotational spectrum.

The timing sequence for pulsed nozzle, ablation laser, and excitation/ionization laser is controlled by time delay generators (SRS DG535). The experiment is run at a repetition rate of 10 Hz. Ion signals in the TOFMS are detected by a microchannel plate (MCP) and signals are recorded and processed on a personal computer (PC) using an ADC (analog to digital converter) card (Analog Devices RTI-800) and a boxcar averager (SRS SR 250).

Since no experimental data exist for vertical excitation energies of  $(NH_4)_2BT$  and TAGzT, in order to determine the accuracy of theoretical calculation for the higher electronic



states, the experimental UV-vis absorption spectra of the two energetic salts are taken with an UV-vis-NIR Varian Cary 500 spectrometer in the range from 182 to 1000 nm. The two samples are dissolved in water with concentrations between  $10^{-6}$  and  $10^{-5}$  mol/l. These spectra are discussed in Section IV.

### III. COMPUTATIONAL METHODS

The calculations for  $(\text{NH}_4)_2\text{BT}$  are executed at the CASSCF(12,8)/6-31G(d) level of theory within the Gaussian 09 program. To explore the excited state potential energy surfaces, the active space comprises 12 electrons distributed in 8 orbitals, denoted as CASSCF(12,8). The equilibrium geometry calculations are conducted taking the total charge as neutral and the spin multiplicity as 1 ( $S = 0$ ). Because the structure of TAGzT is too complicated and using the CASSCF(12,8)/6-31G(d) method takes an extremely long time, a two layered ONIOM (CASSCF/6-31G(d):UFF) method has, therefore, been applied to explore the non-adiabatically coupled ground and excited electronic state potential energy surfaces of the isolated TAGzT molecule.<sup>30</sup> The two triaminoguanidinium cations of TAGzT are considered as the lower layer and the 5,5'-azotetrazolate anion is the higher layer in the ONIOM (CASSCF/6-31G(d):UFF) calculation. For the entire TAGzT molecule (also called “real system” in the ONIOM method), the total charge is neutral and the spin multiplicity is 1 ( $S = 0$ ). For the TAGzT model system, the high layer ( $\text{zT}^{2-}$ ) charge value is  $-2$ , while for the low layer (TAG cations), the charge value equals  $+2$ . The spin multiplicity in the model system in both layers equals 1 ( $S = 0$ ). No symmetry restrictions are applied for the calculations.

The active spaces used in the CASSCF methods for  $(\text{NH}_4)_2\text{BT}$  and TAGzT are presented in Figures 2 and 3. Orbitals used for  $(\text{NH}_4)_2\text{BT}$  are one  $\pi$ -bonding orbital on

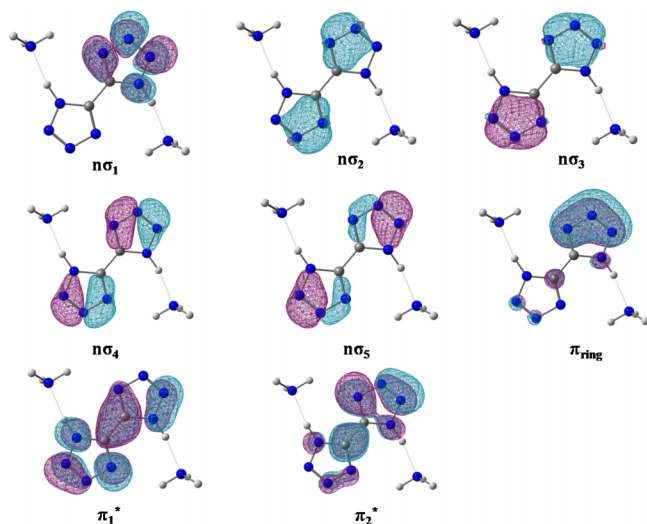


FIG. 2. Orbitals used in the active space of CASSCF(12,8)/6-31G(d) calculations for  $(\text{NH}_4)_2\text{BT}$ . The (12,8) active space comprises one  $\pi$ -bonding orbital on one of the tetrazole rings  $\pi_{\text{ring}}$ , five  $\sigma$ -nonbonding orbitals on two tetrazole rings  $n\sigma_1$ ,  $n\sigma_2$ ,  $n\sigma_3$ ,  $n\sigma_4$ , and  $n\sigma_5$ , and two  $\pi$ -antibonding orbitals on two tetrazole rings  $\pi_1^*$  and  $\pi_2^*$ .

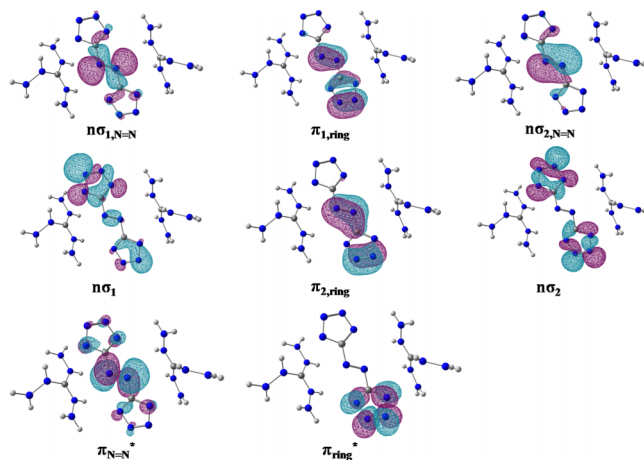


FIG. 3. Orbitals used in the active space of ONIOM (CASSCF/6-31G(d):UFF) calculations for TAGzT. The (12,8) active space comprises two  $\sigma$ -nonbonding orbitals around the  $\text{N}=\text{N}$  bridge between the two tetrazole rings  $n\sigma_{1,\text{N}=\text{N}}$  and  $n\sigma_{2,\text{N}=\text{N}}$ , two  $\pi$ -bonding orbitals around one of the tetrazole rings  $\pi_{1,\text{ring}}$  and  $\pi_{2,\text{ring}}$ , two  $\sigma$ -nonbonding orbitals on the whole molecular system  $n\sigma_1$  and  $n\sigma_2$ , one  $\pi$ -antibonding orbital on the  $\text{N}=\text{N}$  bridge  $\pi_{\text{N}=\text{N}}^*$ , and one  $\pi$ -antibonding orbital on one of the tetrazole ring  $\pi_{\text{ring}}^*$ .

one of the tetrazole rings  $\pi_{\text{ring}}$ , five  $\sigma$ -nonbonding orbitals on two tetrazole rings  $n\sigma_1$ ,  $n\sigma_2$ ,  $n\sigma_3$ ,  $n\sigma_4$ , and  $n\sigma_5$ , and two  $\pi$ -antibonding orbitals on two tetrazole rings  $\pi_1^*$  and  $\pi_2^*$ , as shown in Figure 2. Orbitals used for TAGzT include two  $\sigma$ -nonbonding orbitals around the  $\text{N}=\text{N}$  bridge between the two tetrazole rings  $n\sigma_{1,\text{N}=\text{N}}$  and  $n\sigma_{2,\text{N}=\text{N}}$ , two  $\pi$ -bonding orbitals around one of the tetrazole rings  $\pi_{1,\text{ring}}$  and  $\pi_{2,\text{ring}}$ , two  $\sigma$ -nonbonding orbitals on the whole molecular system  $n\sigma_1$  and  $n\sigma_2$ , one  $\pi$ -antibonding orbital on the  $\text{N}=\text{N}$  bridge  $\pi_{\text{N}=\text{N}}^*$ , and one  $\pi$ -antibonding orbital on one of the tetrazole ring  $\pi_{\text{ring}}^*$ , as shown in Figure 3. For both energetic salts, the dissociation steps involve the opening of one of the tetrazole rings, thus, both  $\sigma$ -nonbonding orbitals and  $\pi$  orbitals around the tetrazole ring are selected for exploration of decomposition mechanisms. The chosen orbitals are mainly molecular orbitals from HOMO-4 to LUMO+2. Eight orbitals are selected because it is the maximum limit for CASSCF for conical intersection calculations due to the need for analytic second derivatives. The agreement between theory and experiment demonstrates that 8 orbitals are sufficient in this instance to derive mechanisms for the initial fragmentation reactions. Excitation energies are calculated by state averaging over the ground and excited states with equal weights for each state. Larger basis sets than 6-31G(d) for CASSCF calculations do not substantially improve the results and understanding of the reaction mechanisms.<sup>15,16</sup>

Critical points (minima and transition state structures) are characterized by analytical frequency calculations, and minimum energy paths are calculated using an intrinsic reaction coordinate (IRC) algorithm implemented in the Gaussian 09 program suite. To find transition and intermediate states along reaction pathways, a relaxed scan optimization algorithm as implemented is employed in which all geometrical parameters except for the specified bond distance are optimized and electronic energies are monitored as the specified bond is elongated. The bond length increase for each

step is 0.1 angstrom for a total scan length of 3.0 angstroms. The structure with peak potential energy in the scan is most likely a transition state, and the structure with potential energy in a valley is most likely an intermediate state. To verify this conclusion and obtain a more accurate potential energy surface for the transition/intermediate states, the molecular structure provided in the scan is used as the initial structure in an adiabatic optimization calculation at the CASSCF(12,8) level and the given active space.

Accuracy of the calculations along the reaction pathway is difficult to estimate since experimental information about conical intersections and transition states is not available. Calculations presented in this paper, however, are based on the experimental observations including the decomposition product  $N_2$  and its internal energy distribution. Thus, the proposed reaction pathways/mechanisms, based on the computational results, provide a reasonable, and at minimum qualitative, interpretation for the experimental observations.

## IV. EXPERIMENTAL RESULTS AND DISCUSSION

### A. UV-vis absorption spectra of $(NH_4)_2BT$ and TAGzT

The UV-vis absorption spectra for  $(NH_4)_2BT$  and TAGzT are shown in Figure 4: the maximum absorption wavelengths in the experimental range for  $(NH_4)_2BT$  are 185 and 215 nm. For TAGzT, a weak absorption feature is found at 422 nm and another two strong absorption peaks are located at 309 nm and 186 nm. In the decomposition study, the laser wavelength is 283 nm, and a two photon absorption process occurs for the decomposition of  $(NH_4)_2BT$ ; one photon absorption and two photon absorption will occur for TAGzT at the 283 nm excitation wavelength. As  $N_2$  detection is a one color, (2 + 2), resonance-enhanced, four photon ionization (REMPI) process, the laser energy/pulse is ca. 20 times greater than that employed for (1 + 1) REMPI detection, such as employed for NO detection. The overall excitation/ $N_2$  detection process for  $(NH_4)_2BT$  and TAGzT salts is thereby a five or six photon process.

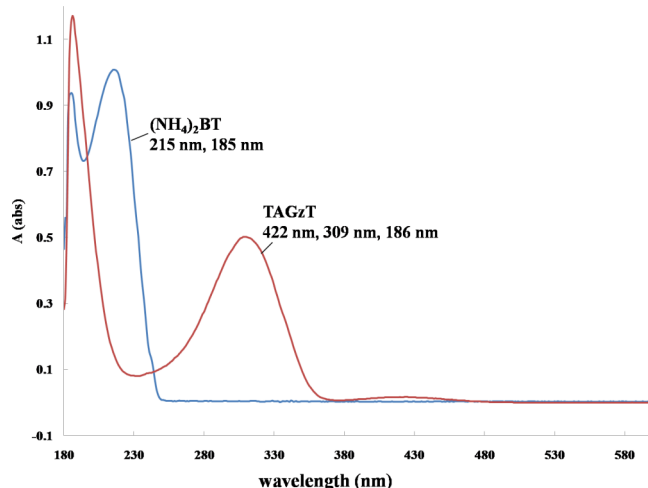


FIG. 4. UV-vis absorption spectra of  $(NH_4)_2BT$  and TAGzT with maximum absorption wavelengths. The energetic salts are dissolved in distilled water.

### B. Decomposition product $N_2$

Decomposition product  $N_2$  is observed from electronically excited  $(NH_4)_2BT$  and TAGzT compounds employing 283 nm excitation and TOFMS detection. The 283 nm excitation wavelength corresponds to the resonance (1-0) vibronic band of the  $a^1\Pi_g \leftarrow X^1\Sigma_g$  electronic transition of the  $N_2$  product.<sup>47–49</sup> REMPI (2 + 2) rotationally resolved spectra of the  $N_2$  product from the two energetic salts are obtained by scanning the laser excitation wavelength. The line width of the  $N_2$  mass peak is 10 ns (~laser pulse width) and laser beam intensity is varied without change in the  $N_2$  TOFMS line width or spectral features. The hot energetic molecules, which might be generated in the ablation process, are effectively relaxed and cooled in the highly collisional expansion process, through the supersonic expansion. Additionally, the 532 nm ablation laser is not directly resonant for the energetic salts and these photons are almost completely absorbed by the R6G matrix. The two energetic salts have a very low absorption at 532 nm (2.33 eV): their higher electronic states are roughly 2-3 eV above this ablation photon energy. In the ablation process, energetic materials can be heated to higher rovibrational states of the electronic ground state. These intact energetic molecules are then cooled in the supersonic expansion. Based on our previous studies, decomposition of such energetic molecules under 532 nm laser irradiation is below our detection limit.<sup>13</sup>

Figure 5 shows the spectra of  $a^1\Pi_g(v' = 1) \leftarrow X^1\Sigma_g(v'' = 0)$  rovibronic transition of the  $N_2$  molecule arising from a 3%  $N_2/He$  mixture, and energetic salts  $(NH_4)_2BT$  and TAGzT following excitation to their excited electronic states. The rotational spectra of  $N_2$  from the  $N_2$  gas mixture and the two energetic salts have similar patterns: the most intense peak in each spectrum of  $N_2$  corresponds to the  $S_0$  peak of the S branch rotational transitions. Other peaks, including  $S_1$  and  $S_2$  of the S branch,  $Q_1$  peak of the Q branch, and  $P_2$  peak of the P branch rotational transitions are labeled in

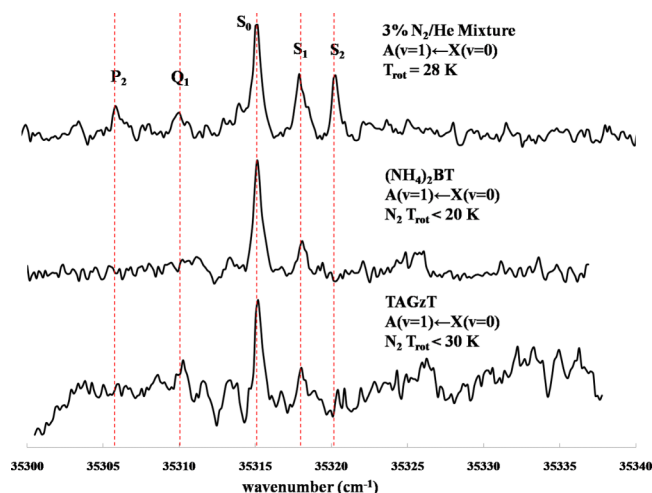


FIG. 5. One color (2 + 2) REMPI spectra of the vibronic transitions  $a^1\Pi_g(v' = 1) \leftarrow X^1\Sigma_g(v'' = 0)$  of  $N_2$  from 3%  $N_2/He$  mixture, and from electronic state excitation of  $(NH_4)_2BT$  and TAGzT. The rotational temperature of the 3%  $N_2$  mixture calculated from a Boltzmann plot equals 28 K. The rotational temperatures of  $N_2$  decomposition products from  $(NH_4)_2BT$  and TAGzT (as indicated) are estimated to be smaller than 30 K.

Figure 5.<sup>47–49</sup> The rotational spectrum of  $N_2$  from  $(NH_4)_2BT$  clearly evidences two peaks of the S branch:  $S_0$  and  $S_1$ . The rotational transition signals of  $N_2$  from TAGzT are much weaker, and only the strongest  $S_0$  peak is identified, as other peaks are too close to the background noise. The rotational spectrum for the  $N_2$ /He mixture and  $(NH_4)_2BT$  expansions is similar to that of previous studies, indicating an  $N_2$  rotational temperature of about 20 K.<sup>16,17,47–50</sup> The  $N_2$  signals from TAGzT are much less intense and, through the comparison to the  $N_2$  gas spectra in different rotational temperatures in previous studies,<sup>16,17,47–50</sup> the rotational temperature of the  $N_2$  product released from the TAGzT salt is assigned as lower than 30 K.

To find the vibrational temperature of the  $N_2$  initial fragmentation product, the rotational spectra of  $N_2$  should be obtained from several vibronic bands. The signal intensity of the reported  $N_2$  rotational transition from ground rovibronic state  $v'' = 0$  is ca. 100 mV, about 5 times higher than the noise level. To get  $N_2$  rovibronic transition spectra starting at  $v'' \geq 1$  of the ground electronic state, the signal intensity should be 5–10 times lower than the above 100 mV, assuming an established vibrational temperature, as is typical for such fragmentation processes.<sup>12–27</sup> This estimated transition intensity is well under the detection limit for the measurement. Consequently, further  $N_2$  rovibronic bands were not obtained in these experiments, and thus vibrational temperature is not determined for the  $N_2$  products of  $(NH_4)_2BT$  and TAGzT.

TOF mass spectra, obtained under 283 nm excitation employed especially for  $N_2$  detection, display a few very weak additional features in the low mass region. These features are, however, much weaker and their intensity remains constant as the excitation wavelength is scanned. These additional weak features are most likely not a result of a major decomposition pathway from the energetic salts.

## V. THEORETICAL RESULTS AND DISCUSSION

### A. Structures of $(NH_4)_2BT$ and TAGzT and their excitation energies

The ground state structure of  $(NH_4)_2BT$  at the CASSCF(12,8)/6-31G(d) calculational level is planar for the bistetrazole rings with a torsion dihedral angle  $N5-C1-C1'-N5'$  of  $179.977^\circ$  (labels in Figure 1). The calculated N—N bond lengths in the tetrazole ring of  $(NH_4)_2BT$  are from 1.257 Å to 1.334 Å, which are between the N—N single bond (1.48 Å) and N=N double bond (1.20 Å).<sup>4</sup> The ring C—N bond length in  $(NH_4)_2BT$  is 1.325 Å, which lies between the C—N single bond (1.47 Å) and C=N double bond (1.22 Å).<sup>4</sup> The C—C bond connecting the two tetrazole rings is 1.458 Å, which is shorter than the typical C—C single bond (1.54 Å).<sup>4</sup> All the geometric values are close to the previous calculations of the  $(NH_4)_2BT$  crystal in the monoclinic space group C2m structure and other bistetrazole derivatives.<sup>4,6</sup> The comparison of the  $(NH_4)_2BT$  dianion structural parameters between the gas phase and the condensed phase from the previous study is summarized in Table I. From Table I, it is found that the bond length difference in the two different phases is within 0.06 Å and the bond angle difference is within  $3.2^\circ$ . These

TABLE I. Comparison of the  $(NH_4)_2BT$  dianion structural parameters between the gas and condensed phase in the previous study. The labels of the atoms are shown in Figure 1.

$(NH_4)_2BT$	Gas phase	Condensed phase <sup>a</sup>
N—C	1.296, 1.325	1.334
N2—N3/N4—N5	1.318, 1.334	1.342
N3—N4	1.257	1.314
C—C	1.458	1.461
N2—C1—N5	108.5	112.1
N3—N2—C1/N4—N5—C1	105.6, 107.6	104.4
N3—N4—N5/N5—N4—N3	110.9, 107.4	109.6
N5—C1—C1'/N2—C1—C1'	125.1, 126.4	123.9

<sup>a</sup>Reference 4.

differences are caused by the increased number of hydrogen bonds in the  $(NH_4)_2BT$  crystal. The crystal structure analysis suggests a hydrogen bond network is formed among the cations and dianions.<sup>4</sup> In the present calculation, for the gas phase ground state Frank Condon structure of  $(NH_4)_2BT$ , both negative N atoms in the bistetrazole dianion are bonded to hydrogen atoms of the  $NH_4$  moiety and form a  $H_3N...H—N—R$  structure (R = rest of tetrazole ring). This structure is similar to that found for the energetic salts TKX-50 and MAD-X1.<sup>16</sup> The structure of isolated  $(NH_4)_2BT$  calculated by the CASSCF(12,8)/6-31G(d) method is shown in Figure 6. The hydrogen bond N...H distance between the N atom of the ammonium moiety and its H atom coordinated to the tetrazole ring is 1.892 Å, and the H—N bond to the tetrazole ring is 1.021 Å in length, 0.018 Å longer than the N—H bond of the  $NH_3$  moiety. The calculated structure for  $(NH_4)_2BT$  depicted in Figure 6 represents an almost complete proton transfer, generating a molecular complex of the form  $(NH_3)_2(H_2BT)$ . Unlike the crystal, in the gas phase, the isolated  $(NH_4)_2BT$  molecule does not have a strict cation-anion salt structure, but rather appears more as a hydrogen bonded compound: this is not a very surprising result as based on previous studies of energetic salt crystals, the energy barrier for proton transfer from cation to anion is ca. 10 kcal/mol.<sup>34</sup> The molecular species is, however, calculated as a whole system, including all

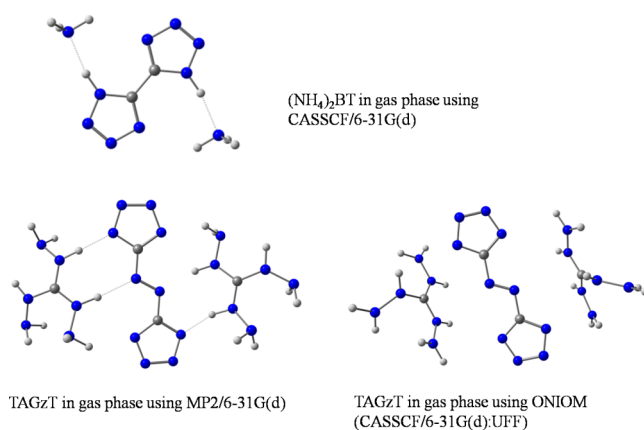


FIG. 6. Top: Structure of isolated  $(NH_4)_2BT$  molecule in the gas phase through CASSCF(12,8)/6-31G(d) calculation. Bottom: Structures of isolated TAGzT molecule in the gas phase through MP2/6-31G(d) and ONIOM (CASSCF/6-31G(d):UFF) calculations, respectively.



the hydrogen bonds between the two  $\text{NH}_4$  cation moieties and the dianion bistetrazole rings. Nonetheless, decomposition of  $(\text{NH}_4)_2\text{BT}$  creating the  $\text{N}_2$  observed in the experiment occurs within its tetrazole ring; thus, the types of bonds between the  $\text{NH}_4$  groups and bistetrazole rings are not the main issue or concern for this study, as long as the appropriate electronic and geometric structures are considered. The hydrogen bonding patterns are similar for the crystal. The essential point is that, in both gas and condensed phase, electronic excitation is the main issue for the bistetrazole moiety decomposition.

The TAGzT MP2/6-31G(d) structure obtained is also shown in Figure 6: the azotetrazolate dianion has a planar structure with a torsion dihedral angle  $\text{C1}-\text{N}=\text{N}-\text{C1}'$  of  $178.601^\circ$  (labels in Figure 1). The  $\text{N}-\text{N}$  bonds of the tetrazole ring are between 1.340 and 1.358 Å and the  $\text{N}=\text{N}$  bond of the bridge between the two tetrazole rings is 1.289 Å. The  $\text{C}-\text{N}$  bonds on the tetrazole ring are between 1.348 and 1.351 Å. For  $\text{C}-\text{N}=\text{N}-\text{C}$  bridge,  $\text{C}-\text{N}$  bonds are a little longer at 1.386 to 1.387 Å. All these bonds have double bond character as a result of  $\pi$ -electron delocalization, consistent with results of previous studies.<sup>1,2,9</sup> For the triaminoguanidinium cations  $\text{C}(\text{NHNH}_2)_3^+$ , the dihedral angle among the carbon in the center and three nitrogen atoms surrounding it is in the range  $1.475^\circ$ – $2.699^\circ$ , and these heavy atoms are nearly co-planar, in agreement with previous results.<sup>9</sup> Two of the three H atoms in the NH structure of  $\text{C}(\text{NHNH}_2)_3^+$  participate in the intramolecular hydrogen bonds with N atoms: one on the tetrazole ring and the other on the  $\text{N}=\text{N}$  bridge. Because the structure of TAGzT is complicated with many atoms and the CASSCF(12,8)/6-31G(d) method becomes very costly, a two layered ONIOM (CASSCF/6-31G(d):UFF) method has been applied to its structure, as shown in Figure 6. The azotetrazolate dianion is in the high layer, while the two triaminoguanidinium cations comprise the low layer. Similar to the MP2/6-31G(d) structure, a planar structure, with the torsion dihedral angle  $\text{C1}-\text{N}=\text{N}-\text{C1}'$  of  $179.137^\circ$ , is found for the azotetrazolate dianion. The  $\text{N}-\text{N}$  bonds on the tetrazole ring lie between 1.291 and 1.312 Å, about 0.05 Å shorter than found by the MP2 method, and the  $\text{N}=\text{N}$  bond on the bridge is 1.224 Å, 0.07 Å shorter than found by MP2.  $\text{C}-\text{N}$  bonds on the tetrazole rings lie between 1.320 and 1.321 Å, 0.03 Å shorter than found by the MP2 method. The  $\text{C}-\text{N}=\text{N}-\text{C}$  bridge has  $\text{C}-\text{N}$  bonds of 1.411 Å, 0.03 Å longer than found by the MP2 method. For triaminoguanidinium cations  $\text{C}(\text{NHNH}_2)_3^+$ , the structure is still nearly co-planar; however, no obvious intramolecular H-bonds are suggested between the cation and azotetrazolate dianion. The absence of the anion/cation H-bonds is perhaps the main reason for the bond length differences between the MP2 and ONIOM (CASSCF/6-31G(d):UFF) methods; however, since all these  $\text{N}-\text{N}$  and  $\text{C}-\text{N}$  bonds still show both single and double bond character, this latter approximation is employed in order to calculate the potential energy surfaces for the ground and first excited states. To test the accuracy and applicability of the ONIOM method, an ONIOM approach is applied to  $(\text{NH}_4)_2\text{BT}$ , as well: the results of these calculations are compared to the CASSCF approach and presented in the supplementary material.<sup>55</sup> The ONIOM algorithm, appropriately partitioned, can provide

a qualitative and reasonable picture of the decomposition mechanism, although not all the energies of the critical points are accurate.

Experimental results yield that the  $\text{N}_2$  molecule is the initial nanosecond electronic excitation decomposition product for the energetic salt systems explored under this study. In order to understand the experimental data more completely and derive reaction mechanisms, theoretical calculations of molecular geometries and energies for the Franck-Condon structures, conical intersections, transition states, and intermediate states along both the ground and excited state potential energy surfaces are explored for both energetic salts. These theoretically derived reaction paths with potential energies and molecular geometries are shown in Figures 7–10.

Four possible decomposition mechanisms are explored for  $(\text{NH}_4)_2\text{BT}$  in the theoretical study, through four different conical intersections between the  $S_1$  and  $S_0$  electronic states, all of which are related to opening of the tetrazole ring. Five possible decomposition mechanisms are explored for TAGzT, including four tetrazole ring opening channels and the breaking of the  $\text{C}-\text{N}$  bond between one tetrazole ring and the  $\text{N}=\text{N}$  bridge. All these reaction channels are chosen because they are energy available and accessible for creation of an  $\text{N}_2$  product. The actual reaction pathways or mechanisms followed by these molecules will depend on different factors, for example, the rate of internal vibrational energy redistribution, the heights of reaction barriers, and the

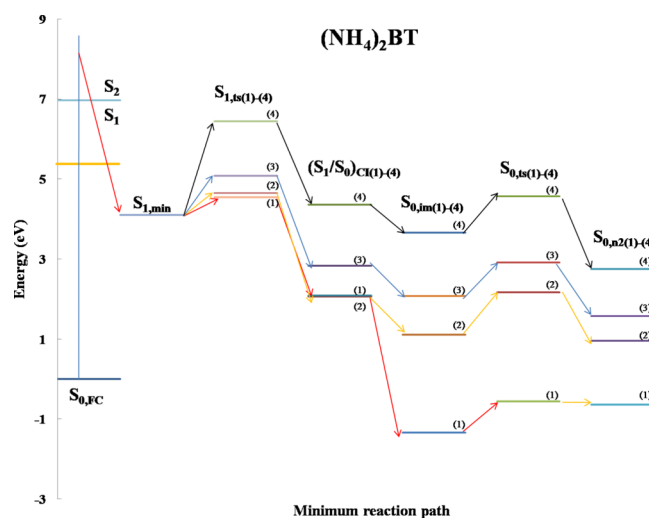


FIG. 7. A schematic one-dimensional projection of the multi-dimensional energy surfaces for four  $(\text{NH}_4)_2\text{BT}$  dissociation paths computed at the CASSCF(12,8)/6-31G(d) level of theory. The four reaction paths contain four tetrazole ring opening channels. The red, orange, blue, and black arrows represent (1)–(4) different reaction channels for  $\text{N}_2$  dissociation, respectively.  $S_{0,\text{FC}}$  is the optimized minimum energy of  $(\text{NH}_4)_2\text{BT}$  on the  $S_0$  state.  $(S_1/S_0)\text{CI}(1)-(4)$  are the conical intersections between the  $S_0$  and  $S_1$  states and (1)–(4) are related to different tetrazole ring opening positions (reactions, minimum energy coordinates) in different reaction channels.  $S_{1,\text{ts}(1)-(4)}$  are the excited transition states on the  $S_1$  electronic state surface between the minimum structure  $S_{1,\text{min}}$  on  $S_1$  and their related conical intersections.  $S_{0,\text{im}(1)-(4)}$  are the intermediate states on the ground electronic state  $S_0$  after  $(S_1/S_0)\text{CI}(1)-(4)$ , and  $S_{0,\text{ts}(1)-(4)}$  are the transition states on the  $S_0$  state following each intermediate state in the different reaction channels.  $S_{0,\text{n2}(1)-(4)}$  are molecules with  $\text{N}_2$  dissociated products on the  $S_0$  state.



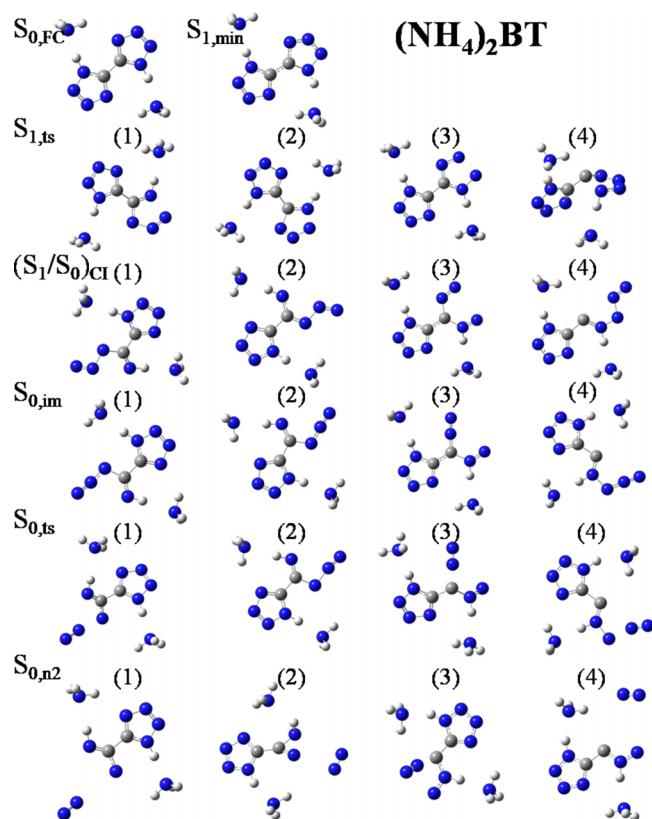


FIG. 8. Structures of all critical points and conical intersections mentioned in Figure 7 along the  $(\text{NH}_4)_2\text{BT}$  dissociation reaction paths (1)–(4). For atoms in the structure, grey is carbon, blue is nitrogen, and white is hydrogen.

rate of non-adiabatic transition through the different conical intersections: at present these dynamics are not individually experimentally accessible.

Calculations at the CASSCF(12,8)/6-31G(d) and ONIOM (CASSCF/6-31G(d):UFF) levels are employed to determine the vertical excitation energies for  $(\text{NH}_4)_2\text{BT}$  and TAGzT from the ground electronic state  $S_0$  (FC structure) to the first and second excited electronic states  $S_1$  and  $S_2$ , respectively. The vertical excitations calculated for the  $S_1$  and  $S_2$  electronic states of  $(\text{NH}_4)_2\text{BT}$  are 5.24 and 6.96 eV. The maximum absorption wavelengths for the  $(\text{NH}_4)_2\text{BT}$  salt in UV-vis absorption spectra shown in Figure 4 are 215 nm (5.77 eV) and 185 nm (6.70 eV). The commonly accepted uncertainty range for CASSCF calculated energies is  $\pm 0.5$  eV;<sup>51,52</sup> calculation of the relevant excited states of  $(\text{NH}_4)_2\text{BT}$  is thus considered reasonable. The vertical excitations calculated for the  $S_1$  and  $S_2$  electronic states of TAGzT are 2.15 and 5.24 eV. The three absorption wavelengths of TAGzT in UV-vis absorption shown in Figure 4 are 422 nm (2.93 eV), 309 nm (4.01 eV), and 186 nm (6.66 eV). The theoretical and experimental difference for TAGzT becomes larger mainly because the ONIOM approximation is used and the cations and dianion of the salt are divided into two layers; however, since we focus on the  $S_1$  and  $S_0$  states of TAGzT, the theoretical result for the TAGzT ( $E_1 - E_0$ ) is still reasonable. Under the chosen experimental conditions for these studies, the molecular excitation for TAGzT is a one or two photon process as the energy of laser excitation in our experiment equals 4.38 eV (283 nm), higher

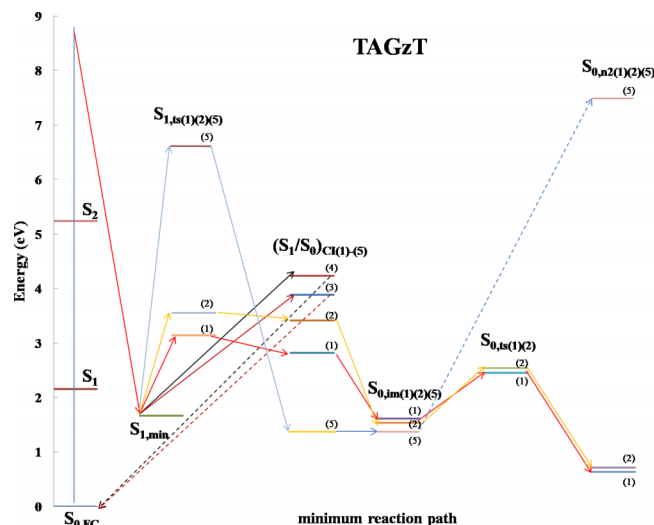


FIG. 9. A schematic one-dimensional projection of the multi-dimensional energy surfaces for five TAGzT dissociation paths computed at the ONIOM (CASSCF/6-31G(d):UFF) level of theory. The five reaction paths contain four tetrazole ring opening channels and one C—N bond opening channel between the tetrazole ring and the N=N bridge. The red, orange, brown, black, and blue arrows represent (1)–(5) different reaction channels for  $\text{N}_2$  dissociation.  $S_{0,\text{FC}}$  is the optimized minimum energy of TAGzT on the  $S_0$  state with a planar structure.  $(S_1/S_0)_{\text{CI}(1)-(5)}$  are the conical intersections between the  $S_0$  and  $S_1$  states and  $S_{1,\text{ts}(1)(2)(5)}$  are the excited transition states on the  $S_1$  surface between the minimum structure  $S_{1,\text{min}}$  and the related conical intersections.  $S_{0,\text{im}(1)(2)(5)}$  are the intermediate states on  $S_0$  after  $(S_1/S_0)_{\text{CI}(1)(2)(5)}$ , and  $(S_1/S_0)_{\text{CI}(3)(4)}$  move back to  $S_{0,\text{FC}}$  after the IRC scan.  $S_{0,\text{ts}(1)(2)}$  are the transition states on the  $S_0$  surface following the related intermediate states and  $S_{0,\text{n2}(1)(2)(5)}$  are  $\text{N}_2$  dissociated products on the  $S_0$  state.

than the  $S_n$  energy of TAGzT ( $n \leq 2$ , from UV spectra): these energetic molecules can thereby be excited to higher electronic states. TAGzT can rapidly ( $< 100$  fs) evolve to the ground electronic potential energy surface through conical intersections between the different electronic states.<sup>12-14,43-46</sup>

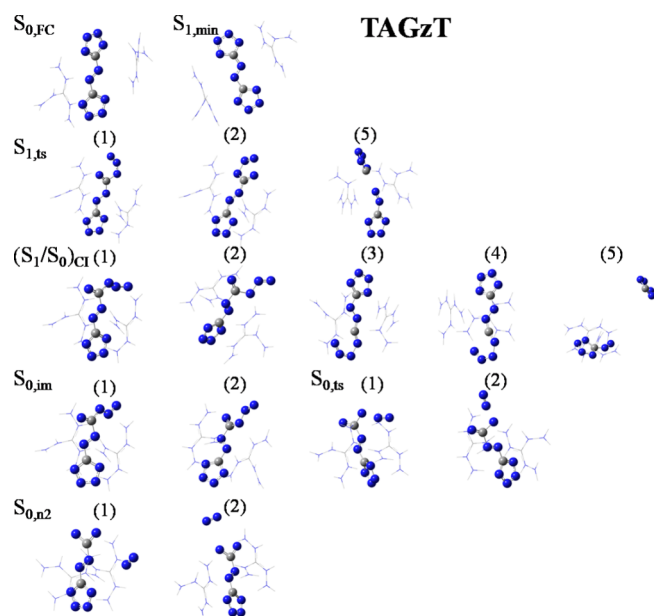


FIG. 10. Structures of all critical points and conical intersections mentioned in Figure 9 along the TAGzT dissociation reaction paths (1)–(5). For atoms in the structure, grey is carbon, blue is nitrogen, and white is hydrogen.



create an  $N_2$  product, the energy barriers in this case will be greater than 3.5 eV; therefore,  $(NH_4)_2BT$  is more likely to open a tetrazole ring on the first excited state  $S_1$  and then move to the  $S_0$  state through various conical intersections. The energies of the final molecular structure with a dissociated  $N_2$  product in the four reaction paths are in the range from  $-0.64$  to  $2.75$  eV; thus, dissociation products should thereby have high vibrational temperatures as the energy in the molecule from photon absorption is now transferred and stored as vibrational energy on the ground electronic state surface. The  $N_2$  product moves away from the rest of the molecule or radical without obvious torque for all the reaction channels as shown in Figure 8. Therefore,  $N_2$  products should have low rotational temperatures, as is consistent with experimental results.

In sum,  $(NH_4)_2BT$  absorbs two laser photons and is excited from the ground state to higher electronic states. The concomitant electronic excitation models the condensed phase, triboluminescent processes that occur upon shock wave, etc., crystal initiation of the energy release processes. It then decomposes to form  $N_2$  products, following four possible reaction paths, as outlined in Figure 7. The tetrazole ring of  $(NH_4)_2BT$  opens on the first excited state  $S_1$ : the  $N_2$  product is dissociated on the ground electronic potential energy surface. The decomposition dynamics are purely non-adiabatic in nature and conical intersections lead rapidly and efficiently to internal conversion from upper to lower electronic states through non-adiabatic, radiationless transitions. During this internal conversion, electronic energy in the upper state is converted to vibrational energy on the lower states in a potential time scale of a few tens of femtoseconds. The difference between the excited state energy  $S_n$  of  $(NH_4)_2BT$  ( $S_n$  is an excited electronic state which the laser energy can reach,  $n > 2$  in this study) and the energy of the final decomposition structure with an  $N_2$  dissociated product plus their internal energies is the energy released from the  $(NH_4)_2BT$  salt in this initial molecular step. Based on our calculations,  $N_2$  should have a high vibrational temperature. This conclusion is consistent with all the energetic materials we have studied previously,<sup>12–27</sup> independent of the small molecule NO or  $N_2$  dissociated product from the energetic molecule. In condensed phase, the explosion involves a chain reaction: this further reaction chain is not directly incorporated into the isolated molecule initial reaction mechanism; nonetheless, any condensed phase chain reaction certainly depends upon the initial molecular mechanism and dynamics. Under a high vibrational temperature, the energetic material can continue to perform secondary decomposition reactions in high density and condensed phase energetic systems.

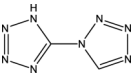
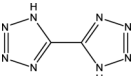
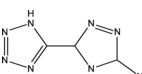
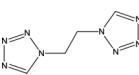
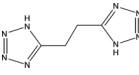
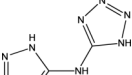
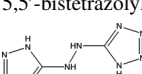
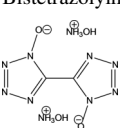
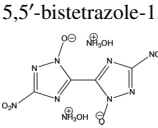
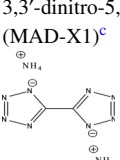
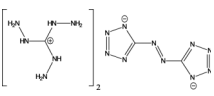
Table III summarizes all the tetrazole-based, nitrogen-rich energetic materials studied in our laboratory, including seven normal organic molecules and four salts.<sup>16,17,54</sup> Similar to previous studies of nitrogen-rich energetic materials based on the tetrazole ring (1,5'-BT, 5,5'-BT, 1-DTE, 5-DTE, BTA, BTH) without an  $NO_2$  or  $N_2O_2$  group or other functional groups, such as  $N_3$ , the tetrazole ring must open in order to form an initial  $N_2$  product. The conclusion “on the first excited state surface  $S_1$ , the N—N bond (especially the N—N bond next to the C—N bond) of the tetrazole ring is less

energy expensive to break than is the C—N bond,”<sup>54</sup> not only applies to the tetrazole-based neutral organic molecules, but also agrees with the theoretical results for tetrazole-based energetic salts. Sufficient energy is absorbed by the material in the excitation/decomposition process, such that all ring opening positions for the formation of  $N_2$  are energy available. Among all nitrogen-rich energetic materials we have studied, the lowest energy barriers for the opening of the tetrazole ring are in the range from 0.31 eV to 0.75 eV as shown in Table III: the lowest energy barrier for the opening of tetrazole ring of the  $(NH_4)_2BT$  salt is 0.44 eV. The energy of the final molecular structure with dissociated  $N_2$  product for all the materials listed in Table III is from  $-1.86$  to  $3.11$  eV. For the  $(NH_4)_2BT$  salt, this energy is from  $-0.64$  to  $2.75$  eV, comparable to other nitrogen-rich, neutral organic energetic materials. Additionally, because the  $N_2$  dissociation products being detected have low rotational temperatures ( $<30$  K), all these nitrogen-rich energetic materials, either neutral organic molecules or salts, have similar mechanisms for  $N_2$  dissociation from the tetrazole ring. As shown in Table III, the main difference between energetic salts and neutral organic molecules is that energetic salts have lower excitation energy. Excitation energies to the first excited state  $S_1$  of neutral species are from 6.20 to 7.08 eV, while for energetic salts, TKX-50,  $(NH_4)_2BT$ , and TAGzT (discussed in Sec. V C),  $S_1$ - $S_0$  energy differences are 4.45, 5.24, and 2.15 eV, respectively. Energetic salts have lower excitation energies than their neutral counterparts perhaps due to their extended bonding structure through the anion/cation electronic delocalization, hydrogen bonding, and charge transfer excitations.

### C. Potential energy surfaces for TAGzT

Schematic one-dimensional projections of the multidimensional singlet potential energy surfaces ( $S_0$  and  $S_1$ ) of TAGzT, with locations and potential energies for different critical points and conical intersections along the minimum energy reaction paths, are plotted in Figure 9 and the energy for each point is summarized in Table IV. Figure 9 describes five different reaction mechanisms or channels for TAGzT decomposition, including the opening of tetrazole ring and breaking of the C—N bond connecting the N=N bridge to one of the tetrazole rings. The reaction coordinates depicted in Figure 9 include C—N and N—N bond lengths at the TAGzT active sites. Arrows with colors in red, orange, brown, blue, and black in Figure 9 indicate different possible decomposition channels. Structures at critical points and conical intersections are summarized in Figure 10. In Figures 9 and 10, FC geometry  $S_{0,FC}$  is the optimized minimum energy of TAGzT on  $S_0$ ,  $(S_1/S_0)_{CI(1)-(5)}$  are the conical intersections between the  $S_0$  and  $S_1$  potential energy surfaces, and (1)-(5) relate to the five different decomposition channels.  $S_{1,ts(1)(2)(5)}$  are the excited transition states on the  $S_1$  surface between the minimum structure  $S_{1,min}$  and the related conical intersections. Labels (3) and (4) are missing because a transition state is not located between  $S_{1,min}$  and  $(S_1/S_0)_{CI(3)(4)}$ .  $S_{0,im(1)(2)(5)}$  are the intermediate states on  $S_0$  subsequent to the  $(S_1/S_0)_{CI(1)(2)(5)}$ , and  $S_{0,ts(1)(2)}$  are the transition states on the  $S_0$  surface following the related intermediate states in different reaction channels.

TABLE III. Comparison of energetic salts and neutral organic nitrogen-rich energetic materials. The first column identifies the energetic material considered. The 2nd column shows the energies of excited states on their respective potential energy surface's FC points (vertical excitation). The 3rd and 4th columns show the energies of transition states either for the opening of tetrazole ring or the breaking of other functional groups on the  $S_1$  excited state. In the 3rd and 4th columns, the values in the parenthesis are the energy barriers on the  $S_1$  state: these values equal the energies of the transition states  $S_{1,ts}$  minus the energies of the minimum structures  $S_{1,min}$ . The fifth column shows the energies of the final molecules with dissociated  $N_2$  products on the ground electronic state  $S_0$ . The last column shows the rotational temperatures of  $N_2$  products.

	Excited state $S_1$ , $S_2$ (eV)	Tetrazole ring opening on the $S_1$ state (eV)	Other reaction path forming $N_2$	Final molecule with $N_2$ product (eV)	$T_{rot}(N_2)$
 1,5'-bistetrazole (1,5-BT) <sup>a</sup>	6.26, 7.34	4.81 (0.56) to 5.98 (1.73)	N/A	−0.44 to 2.53	<30
 5,5'-bistetrazole (5,5'-BT) <sup>a</sup>	6.27	4.99 (0.75) to 6.68 (2.44)	N/A	1.33 to 3.11	<30
 Azidotriazolyl-tetrazole (AzTT) <sup>a</sup>	6.20	5.35 (3.61) to 6.49 (4.75)	From N3, 1.95 (0.21)	0.52 to 2.13	<30
 1,1'-ditetrazolyethane (1-DTE) <sup>b</sup>	6.42, 7.22	5.80 (0.31) to 7.06 (1.57)	N/A	−0.98 to 2.18	<20
 5,5'-ditetrazolyethane (5-DTE) <sup>b</sup>	7.08, 7.51	4.57 (0.64) to 5.16 (1.23)	N/A	−1.49 to −0.30	<30
 5,5'-bistetrazolylamine (BTA) <sup>b</sup>	6.49, 7.25	6.11 (0.55) to 6.60 (1.04)	N/A	−1.44 to 0.78	<20
 Bistetrazolylhydrazine (BTH) <sup>b</sup>	6.57, 7.30	6.29 (0.51) to 6.94 (1.17)	N/A	−1.86 to 3.01	<30
 Dihydroxylammonium 5,5'-bistetrazole-1,1'-diolate (TKX-50) <sup>c</sup>	4.45, 4.85	3.99 (0.43) to 4.45 (0.89)	N/A	−1.35 to −0.11	<30
 Dihydroxylammonium 3,3'-dinitro-5,5'-bis-1,2,4-triazole-1,1'-diol (MAD-X1) <sup>c</sup>	...	...	...	−0.48	<30
 Bis(ammonium) 5,5'-bistetrazolate (( $NH_4$ ) <sub>2</sub> BT)	5.24, 6.96	4.54 (0.44) to 6.44 (2.34)	N/A	−0.64 to 2.75	<20
 Bis(triaminoguanidinium) 5,5'-azotetrazolate (TAGzT)	2.15, 5.24	2.66 (1.47) to 4.23 (2.71)	From N=N link, 7.30 eV on $S_0$	0.63 to 0.71	<30

<sup>a</sup>Reference 17.<sup>b</sup>Reference 54.<sup>c</sup>Reference 16.



TABLE IV. Summary of reaction paths and critical point energies for the TAGzT decomposition reaction.

Reaction path	Color	$S_{1,ts}$	$(S_1/S_0)_{CI}$	$S_{0,im}$	$S_{0,ts}$	$S_{0,n2}$
1	Red	3.14	2.82	1.62	2.45	0.63
2	Orange	3.54	3.41	1.53	2.54	0.71
3	Brown	...	3.88		(Back to $S_{0,FC}$ )	
4	Black	...	4.23		(Back to $S_{0,FC}$ )	
(5)	Blue	4.38	0.86	0.85		7.30
Details of each reaction Path (i = 1-4)						
i = 1-2		$S_{1,min} \rightarrow S_{1,ts(i)} \rightarrow (S_1/S_0)_{CI(i)} \rightarrow S_{0,im(i)} \rightarrow S_{0,ts(i)} \rightarrow S_{0,n2(i)}$				
i = 3-4		$S_{1,min} \rightarrow (S_1/S_0)_{CI(i)} \rightarrow S_{0,FC}$				
i = 5		$S_{1,min} \rightarrow S_{1,ts(i)} \rightarrow (S_1/S_0)_{CI(i)} \rightarrow S_{0,im(i)}$				

$S_{0,n2(1)(2)(5)}$  are  $N_2$  dissociated products on the  $S_0$  potential energy surface.

The reaction paths in Figure 9 show that, with one or two photon absorption, TAGzT can be excited to its  $S_n$  ( $n \geq 2$ ) state and then evolve to the first excited electronic state  $S_1$  through several conical intersections. On the  $S_1$  state, TAGzT undergoes a rapid internal conversion to the energy minimum structure  $S_{1,min}$ . Next, the molecular evolution encounters energy barriers to transition states  $S_{1,ts(1)(2)(5)}$  as the molecule passes to the ground electronic state through the  $(S_1/S_0)_{CI(1)-(5)}$  conical intersections: molecules undergoing this process place sufficient vibrational energy in the  $S_0$  state, transferred from the  $S_n$  electronic excitation energy, to dissociate. No transition state is found between  $S_{1,min}$  and  $(S_1/S_0)_{CI(3)(4)}$ ; therefore, on these two reaction paths, the molecule encounters the energy barrier, and moves from  $S_{1,min}$  to the conical intersections  $(S_1/S_0)_{CI(3)(4)}$  directly and then passes to the ground electronic state. The five conical intersections between the  $S_1$  and  $S_0$  potential energy surfaces contain four different tetrazole ring opening positions and the cleavage of the C—N bond between the tetrazole ring and the N=N bridge. The energy barriers from  $S_{1,min}$  to the related transition states (reaction paths (1) (2) (5)) or conical intersections (reaction paths (3) and (4)) are from 1.47 to 2.71 eV. Among these five channels, the breaking of the N2—N3 bond on the tetrazole ring (reaction path (1), red in Figure 9) has the lowest energy barrier. For the opening of the tetrazole ring, the breaking of the C1—N5 bond (reaction path (4), black in Figure 9) has the highest energy barrier (2.56 eV). This theoretical result is consistent with those for previous nitrogen-rich energetic materials we have studied: breaking the C—N bond on the tetrazole ring has a higher energy barrier than breaking an N—N bond on the tetrazole ring. Breaking the C—N bond between the tetrazole ring and the N=N bridge has a still higher energy barrier (2.71 eV) than that for any tetrazole ring opening. The adiabatic energy gaps between the  $S_1$  and  $S_0$  surfaces near  $(S_1/S_0)_{CI(1)-(5)}$  are computed to be in the range between 26 and 395  $cm^{-1}$ ; therefore, the  $S_1$  and  $S_0$  adiabatic surfaces are strongly non-adiabatically coupled with one another: small energy gaps increase the probability of a non-adiabatic transition from upper to lower electronic states.

As the molecule transfers from the  $S_1$  to  $S_0$  surface through  $(S_1/S_0)_{CI(1)-(5)}$ , the steepest descent pathways for the molecule

are evolution to either the stable intermediate states  $S_{0,im(1)(2)(5)}$  or to the Frank-Condon structure  $S_{0,FC}$ . Based on the IRC scan, the tetrazole rings close on the ground electronic state through conical intersections  $(S_1/S_0)_{CI(3)(4)}$  and the molecule returns to the Frank-Condon structure. The tetrazole rings at intermediate states  $S_{0,im(1)(2)}$  along reaction paths (1) and (2), however, stay open. From  $S_{0,im(1)(2)}$  the molecule surmounts energy barriers from 0.83 to 1.00 eV through the concerted transition states  $S_{0,ts(1)(2)}$  and forms  $N_2$  products  $S_{0,n2(1)(2)}$ .  $N_2$  product moves away from the remaining molecule without obvious torque in these two reaction channels as shown in Figure 10. Therefore,  $N_2$  products should have low rotational temperatures, as is consistent with the experimental results. Energies of the final molecules with dissociated  $N_2$  from these two reaction paths are 0.63—0.71 eV. Therefore, most of the electronic energy absorbed through the excitation process is stored as vibrational energy in the molecular system: based on the calculations, the  $N_2$  product should have a high vibrational temperature. From the intermediate state  $S_{0,im(5)}$ , in which the C—N bond between the tetrazole ring and the N=N bridge is broken, to get the dissociated  $N_2$  product, an energy barrier 7.30 eV must be surmounted: this barrier is probably too high to be a competitive open channel (not shown in Figure 9). To open the tetrazole ring on the ground electronic state from Frank Condon structure  $S_{0,FC}$ , the energy barriers are from 3.79 to 4.31 eV, which is about 3 eV higher than those for the opening of the tetrazole ring on the first excited state  $S_1$ . TAGzT is most likely to open a tetrazole ring on its first excited state, with the  $N_2$  molecule dissociated on its ground electronic state.

In sum, TAGzT absorbs one or two laser photons and is electronically excited in the experiment: it undergoes decomposition to form an  $N_2$  product, through two reaction paths as shown in Figure 9. This electronic excitation process is designed to explore the “triboluminescent excitation processes” that occur in the condensed phase electronic excitation through shock wave initiation. Conical intersections are the key features in the excited electronic state chemistry of energetic molecules, including energetic salts. These initial product species, with  $N_2$  product from TAGzT, have relatively high vibrational energy stored in the system for further dissociation reactions. The N—N bond, no matter how the tetrazole rings are connected to each other, is less energy expensive to break than the C—N bond: the tetrazole ring

most likely opens on the first excited state  $S_1$ . Although TAGzT can create  $N_2$  from its  $N=N$  bridge, the tetrazole ring is more reactive for the formation of an  $N_2$  product.

As shown in Table IV, TAGzT has only two reaction paths through which to form  $N_2$  under the current experimental conditions.  $(NH_4)_2BT$ , on the other hand, has four available channels and their energy barriers for the opening of the tetrazole ring on the  $S_1$  state are similar; however, the condensed phase TAGzT is more sensitive<sup>4,9</sup> than  $(NH_4)_2BT$ . The sensitivity of energetic materials has strong dependence on their intermolecular interactions in the condensed phase.<sup>33</sup> Note as well, moreover, TAGzT has lower excitation energy. The first excited state energy of TAGzT is only 2.15 eV, about 3 eV lower than  $(NH_4)_2BT$ . In this case, TAGzT can be much more easily excited in condensed phase initiation processes. The lower excitation energy of TAGzT is probably associated with the extra  $N=N$  double bond between the two tetrazole rings which forms a larger  $\pi$ -delocalization system in the molecule compared to that found for  $(NH_4)_2BT$ . TAGzT, like BTH, can also produce  $N_2$  from the  $N=N$  bridge moiety,<sup>54</sup> however, this mechanism is less reactive, and more energy expensive than opening of the tetrazole ring. This finding is consistent with the decomposition reaction calculated for neutral BTH.<sup>54</sup> A mechanism for  $N_2$  product generation from triaminoguanidinium cations has been studied previously, but  $N_2$  is not suggested to be one of the major products in the initial decomposition step;<sup>1,9</sup> thus, this source is not considered here. TAGzT displays energy barriers for the opening of the tetrazole ring, energy of the final species with dissociated  $N_2$  product, and low rotational  $N_2$  product temperature that fall within a common range for both neutral and salt energetic materials, as shown in Table III. Therefore, except for its lower excitation energy, this energetic salt does not evidence different behavior compared to neutral organic energetic molecules with regard to dissociation of an  $N_2$  molecule.

As a result, the behavior of  $N_2$  dissociation from nitrogen-rich energetic salts  $(NH_4)_2BT$  and TAGzT is consistent with the behavior of neutral energetic compounds reported with a low rotational temperature and a high calculated vibrational temperature.<sup>17,54</sup> The tetrazole ring opens on the first excited state  $S_1$ , and  $N_2$  is created on the ground electronic state  $S_0$ . Conical intersections play an essential role in the decomposition mechanisms. Energy barriers for opening of the tetrazole ring for all these nitrogen-rich energetic molecules and salts are in the range from 0.31 to 2.71 eV, while the energy of the final molecular structure with dissociated  $N_2$  product is from  $-1.86$  to 3.11 eV. In this case, electronic excitation energy is stored as vibrational energy on the ground electronic state surface in the molecular system for further dissociation reactions. The vibrational temperature of the initial dissociation product is important in recognizing energetic molecules because initial decomposition products with high vibrational excitation are better able to propagate a chain reaction following the initial stimulus, leading to detonation. The  $S_n \rightarrow \dots \rightarrow S_0$  pathways through a series of conical intersections leave the molecule on a new part of the  $S_0$  potential energy surface, not necessarily near the FC equilibrium point.<sup>21,22</sup> Thereby, all the excitation energy is available to break internal bonds and to generate reactive

fragments and radicals for further reactions as required to classify a high energy molecule as a potential energetic material.

## VI. CONCLUSIONS

Decomposition of the nitrogen rich energetic salts  $(NH_4)_2BT$  and TAGzT following electronic excitation has been explored. These two energetic salts create  $N_2$  from their tetrazole rings as initial decomposition products through a number of distinct reaction channels, which are similar to those found for tetrazole based neutral energetic organic materials without additional functional groups. The rotational temperature of  $N_2$  products is low ( $<30$  K). Based on the experimental observations and CASSCF calculations for  $(NH_4)_2BT$ , the  $N_2$  product is released by the opening of a tetrazole ring. The tetrazole ring opens on the  $S_1$  excited state surfaces, and through conical intersections  $(S_1/S_0)_{CI}$ ,  $N_2$  products are formed on the ground state surface with little rotational excitation at the last  $N_2$  dissociation step. The tetrazole ring opens at the  $N_2-N_3$  bond with a lower energy barrier than that of the  $C-N$  bond, as is consistent with other tetrazole ring based energetic materials we have studied previously (for example, TKX-50, BTA, BTH, 1-DTE, 5-DTE, 1,5'-BT, and 5,5'-BT).<sup>16,17,54</sup> TAGzT can produce  $N_2$  either by the opening of tetrazole ring or from the  $N=N$  group bridge linking its two tetrazole rings; the opening of the tetrazole ring has lower energy barriers; however, the tetrazole ring opening at the  $N_2-N_3$  bond is the most active position for  $N_2$  formation for both TAGzT and  $(NH_4)_2BT$ . The vibrational temperatures of  $N_2$  products from the two energetic salts should be hot, based on calculations. Conical intersections are the key point for the theoretically derived mechanisms, as they provide non-adiabatic, ultrafast, radiationless internal conversion between upper and lower electronic states on the fs time scale, and place the undissociated molecule on a new part of the ground state potential surface, with all its electronic excitation energy placed in the ground state vibrations available for bond breaking. The energy barriers for the opening of the tetrazole ring for all nitrogen-rich energetic materials studied thus far, including both neutral organic molecules and salts, are in the range from 0.31 to 2.71 eV, while the energy of final molecular structure with dissociated  $N_2$  product ranges from  $-1.86$  to 3.11 eV. The main difference between energetic salt and neutral nitrogen-rich energetic materials is that energetic salts usually have lower excitation energies. Energy of the first excited state  $S_1$  of TKX-50,  $(NH_4)_2BT$ , and TAGzT equals 4.45, 5.24, and 2.15 eV, while for the neutral nitrogen-rich organic materials,  $S_1$  energy is in the range from 6.20 to 7.08 eV.

## ACKNOWLEDGMENTS

This study is supported by a grant from the U.S. Army Research Office (ARO, Grant Nos. FA9550-10-1-0454 and W911-NF13-10192) and in part by the U.S. National Science Foundation (NSF) through the XSEDE supercomputer resources provided by NCSA under Grant No.

TG-CHE110083. We also want to thank Professor Dr. Thomas M. Klapötke, Ludwig-Maximilian University of Munich for supplying the energetic salts  $(\text{NH}_4)_2\text{BT}$  and TAGzT used in this study and for helpful advice on their properties and handling.

- <sup>1</sup>M. Liu, S. Cheng, K. Cheng, and C. Chen, "Kinetics of decomposition pathways of an energetic GZT molecule," *Int. J. Quantum Chem.* **108**, 482 (2008).
- <sup>2</sup>S. Cheng, K. Cheng, M. Liu, Y. Hong, and C. Chen, "Computational study of decomposition mechanisms and thermodynamic properties of molecular-type cracking patterns for the highly energetic molecule GZT," *J. Mol. Model.* **19**, 3705 (2013).
- <sup>3</sup>H. Gao and J. M. Shreeve, "Azole-based energetic salts," *Chem. Rev.* **111**, 7377 (2011).
- <sup>4</sup>N. Fischer, D. Izsak, T. M. Klapötke, S. Rappengluck, and J. Stierstorfer, "Nitrogen-rich 5,5'-bistetrazolates and their potential use in propellant systems: A comprehensive study," *Chem. - Eur. J.* **18**, 4051 (2012).
- <sup>5</sup>K. D. Behler, J. A. Ciezak-Jenkins, and R. C. Sausa, "High-pressure characterization of nitrogen-rich bistriaminoguanidinium azotetrazolate (TAGzT) by *in situ* Raman spectroscopy," *J. Phys. Chem. A* **117**, 1737 (2013).
- <sup>6</sup>L. H. Finger, F. G. Schroder, and J. Sundermeyer, "Synthesis and characterization of 5,5'-bistetrazolate salts with alkali metal, ammonium and imidazolium cations," *Z. Anorg. Allg. Chem.* **639**, 1140 (2013).
- <sup>7</sup>B. C. Tappan, A. N. Ali, and S. F. Son, "Decomposition and ignition of the high-nitrogen compound triaminoguanidinium azotetrazolate (TAGzT)," *Propellants, Explos., Pyrotech.* **31**, 163 (2006).
- <sup>8</sup>N. Fischer, K. Hull, T. M. Klapötke, J. Stierstorfer, G. Laus, M. Hummel, C. Froschauer, K. Wurst, and H. Schottenberger, "5,5'-Azoxytetrazolates—A new nitrogen-rich dianion and its comparison to 5,5'-azotetrazolate," *Dalton Trans.* **41**, 11201 (2012).
- <sup>9</sup>A. Hammerl, M. A. Hiskey, G. Holl, T. M. Klapötke, K. Polborn, J. Stierstorfer, and J. J. Weigand, "Azidoformamidinium and guanidinium 5,5'-azotetrazolate salts," *Chem. Mater.* **17**, 3784 (2005).
- <sup>10</sup>R. V. Tsyshevsky and M. M. Kuklja, "Decomposition mechanisms and kinetics of novel energetic molecules BNFF-1 and ANFF-1: Quantum-chemical modeling," *Molecules* **18**, 8500 (2013).
- <sup>11</sup>D. Yaempongsa, "Quantum chemical studies of new energetic molecules," M.S. thesis in physical chemistry, KTH Kemivertenskap, 2012.
- <sup>12</sup>A. Bhattacharya, Y. Q. Guo, and E. R. Bernstein, "Nonadiabatic reactions of energetic molecules," *Acc. Chem. Res.* **43**, 1476 (2010).
- <sup>13</sup>Y. Q. Guo, A. Bhattacharya, and E. R. Bernstein, "Decomposition of nitramine energetic materials in excited electronic states: RDX and HMX," *J. Chem. Phys.* **122**, 244310 (2005).
- <sup>14</sup>Y. Q. Guo, M. Greenfield, A. Bhattacharya, and E. R. Bernstein, "On the excited electronic state dissociation of nitramine energetic materials and model systems," *J. Chem. Phys.* **127**, 154301 (2007).
- <sup>15</sup>A. Bhattacharya and E. R. Bernstein, "Nonadiabatic decomposition of gas-phase RDX through conical intersections: An ONIOM-CASSCF study," *J. Phys. Chem. A* **115**, 4135 (2011).
- <sup>16</sup>B. Yuan, Z. Yu, and E. R. Bernstein, "Initial mechanisms for the decomposition of electronically excited energetic salts: TKX-50 and MAD-X1," *J. Phys. Chem. A* **119**, 2965 (2015).
- <sup>17</sup>B. Yuan, Z. Yu, and E. R. Bernstein, "Initial mechanisms for the decomposition of electronically excited energetic materials: 1,5'-BT, 5,5'-BT and AzTT," *J. Chem. Phys.* **142**, 124315 (2015).
- <sup>18</sup>A. Bhattacharya, Y. Q. Guo, and E. R. Bernstein, "Unimolecular decomposition of tetrazine-N-oxide based high nitrogen content energetic materials from excited electronic states," *J. Chem. Phys.* **131**, 194304 (2009).
- <sup>19</sup>A. Bhattacharya, Y. Q. Guo, and E. R. Bernstein, "Experimental and theoretical exploration of the initial steps in the decomposition of a model nitramine energetic material: Dimethylnitramine," *J. Phys. Chem. A* **113**, 811 (2009).
- <sup>20</sup>Z. Yu and E. R. Bernstein, "Decomposition of pentaerythritol tetranitrate  $[\text{C}(\text{CH}_2\text{ONO}_2)_4]$  following electronic excitation," *J. Chem. Phys.* **135**, 154305 (2011).
- <sup>21</sup>Z. Yu and E. R. Bernstein, "Experimental and theoretical studies of the decomposition of new imidazole based energetic materials: Model systems," *J. Chem. Phys.* **137**, 114303 (2012).
- <sup>22</sup>Z. Yu and E. R. Bernstein, "On the decomposition mechanisms of new imidazole-based energetic materials," *J. Phys. Chem.* **117**, 1756 (2013).
- <sup>23</sup>Y. Q. Guo, A. Bhattacharya, and E. R. Bernstein, "Decomposition of excited electronic state s-tetrazine and its energetic derivatives," *J. Chem. Phys.* **134**, 024318 (2011).
- <sup>24</sup>Y. Q. Guo, A. Bhattacharya, and E. R. Bernstein, "Excited electronic state decomposition of furazan based energetic materials: 3,3'-diamino-4,4'-azoxyfurazan and its model systems, diaminofurazan and furazan," *J. Chem. Phys.* **128**, 034303 (2008).
- <sup>25</sup>Y. Q. Guo, A. Bhattacharya, and E. R. Bernstein, "Ultrafast S1 to S0 internal conversion dynamics for dimethylnitramine through a conical intersection," *J. Phys. Chem. A* **115**, 9349 (2011).
- <sup>26</sup>B. Yuan, Z. Yu, and E. R. Bernstein, "Azole energetic materials: Initial mechanisms for the energy release from electronical excited nitropyrazoles," *J. Chem. Phys.* **140**, 034320 (2014).
- <sup>27</sup>B. Yuan, Z. Yu, and E. R. Bernstein, "Initial decomposition mechanism for the energy release from electronically excited energetic materials: FOX-7 (1,1-diamino-2,2-dinitroethene,  $\text{C}_2\text{H}_4\text{N}_4\text{O}_4$ )," *J. Chem. Phys.* **140**, 074708 (2014).
- <sup>28</sup>F. J. Owens, "Calculation of energy barriers for bond rupture in some energetic molecules," *J. Mol. Struct.: THEOCHEM* **370**, 11 (1996).
- <sup>29</sup>D. Furman, R. Kosloff, F. Dubnikova, S. V. Zybin, W. A. Goddard III, N. Rom, B. Hirshberg, and Y. Zeiri, "Decomposition of condensed phase energetic materials: Interplay between uni- and bimolecular mechanisms," *J. Am. Chem. Soc.* **136**, 4192 (2014).
- <sup>30</sup>F. M. Nareetisel, *Solventless Isomerisation Reactions of Six-Coordinate Complexes of Ruthenium and Molybdenum, Solid State Reactions* (Ph.D. thesis, Department of Chemistry, University of Witwatersrand, 2006), Chap. II. Online version: <http://wiredspace.wits.ac.za/bitstream/handle/10539/1654/Chapter%202-%20Final.pdf?sequence=2&isAllowed=y>.
- <sup>31</sup>J. Zhang, L. A. Mitchell, D. A. Parrish, and J. M. Shreeve, "Enforced layer-by-layer stacking of energetic salts towards high-performance insensitive energetic materials," *J. Am. Chem. Soc.* **137**, 10532 (2015).
- <sup>32</sup>J. Zhang, Q. Zhang, T. T. Vo, D. A. Parrish, and J. M. Shreeve, "Energetic salts with  $\pi$ -stacking and hydrogen-bonding interactions lead the way to future energetic materials," *J. Am. Chem. Soc.* **137**, 1697 (2015).
- <sup>33</sup>A. L. Ramaswamy, "Microscopic initiation mechanisms in energetic material crystals," *J. Energ. Mater.* **2**, 195 (2001).
- <sup>34</sup>Q. An, W.-G. Liu, W. A. Goddard III, T. Cheng, S. V. Zybin, and H. Xiao, "Initial steps of thermal decomposition of dihydroxylammonium 5,5'-bistetrazole-1,1'-diolate crystals from quantum mechanics," *J. Phys. Chem. C* **118**, 27175 (2014).
- <sup>35</sup>D. D. Dlott and M. D. Fayer, "Shocked molecular solids: Vibrational up-pumping, defect hot spot formation, and the onset of chemistry," *J. Chem. Phys.* **92**, 3798 (1990).
- <sup>36</sup>G. E. Hardy, J. C. Baldwin, J. I. Zink, W. C. Kaska, P.-H. Liu, and L. Dubois, "Triboluminescence spectroscopy of aromatic compounds," *J. Am. Chem. Soc.* **99**, 3533 (1977).
- <sup>37</sup>J. I. Zink and W. C. Kaska, "Triboluminescence of Hexaphenylcarbodi-phosphorane: Emission from a molecular excited state populated by mechanical stress," *J. Am. Chem. Soc.* **95**, 7510 (1973).
- <sup>38</sup>J. I. Zink, G. E. Hardy, and J. E. Sutton, "Triboluminescence of sugars," *J. Phys. Chem.* **80**, 248 (1976).
- <sup>39</sup>J. I. Zink and W. Klimt, "Triboluminescence of coumarin. Fluorescence and dynamic spectral features excited by mechanical stress," *J. Am. Chem. Soc.* **96**, 4690 (1974).
- <sup>40</sup>W. Beese and J. I. Zink, "Intensity of triboluminescence," *J. Lumin.* **29**, 119 (1984).
- <sup>41</sup>G. E. Hardy and J. I. Zink, "Triboluminescence and pressure dependence of the photoluminescence of tetrahedral manganese (II) complexes," *Inorg. Chem.* **15**, 3061 (1976).
- <sup>42</sup>S. H. Lin, D. Wutz, Z. Z. Ho, and H. Eyring, "Mechanisms of triboluminescence," *Proc. Natl. Acad. Sci. U. S. A.* **77**, 1245 (1980).
- <sup>43</sup>M. M. Kuklja, "Role of electronic excitations in explosive decomposition of solids," *J. Appl. Phys.* **89**, 4156 (2001).
- <sup>44</sup>E. J. Reed, J. D. Joannopoulos, and L. E. Fried, "Electronic excitations in shocked nitromethane," *Phys. Rev. B* **62**, 16500 (2000).
- <sup>45</sup>K. Takatsuka, T. Yonehara, K. Hanasaki, and Y. Arasaki, *Chemical Theory Beyond the Born-Oppenheimer Paradigm: Nonadiabatic Electronic and Nuclear Dynamics in Chemical Reactions* (World Scientific Publishing Co. Pte. Ltd, Singapore, 2015).
- <sup>46</sup>W. Domcke, D. R. Yarkony, and H. Koppel, *Conical Intersections: Electronic Structure, Dynamics & Spectroscopy*, Advanced Series in Physical Chemistry Vol. 15 (World Scientific Publishing Co. Pte. Ltd, Singapore, 2004).
- <sup>47</sup>K. L. Carleton, K. H. Welge, and S. R. Leone, "Detection of nitrogen rotational distributions by resonant 2+2 multiphoton ionization through the  $a^1\Pi_g$  state," *Chem. Phys. Lett.* **115**, 492 (1985).

- <sup>48</sup>G. O. Sitz, A. C. Kummel, and R. N. Zare, "Population and alignment of N<sub>2</sub> scattered from Ag(111)," *J. Vac. Sci. Technol., A* **5**, 513 (1987).
- <sup>49</sup>F. J. Aoiz, L. Banares, V. J. Herrero, B. Martinez-Haya, M. Menendez, P. Quintana, L. Tanarro, and E. Verdasco, "Low-temperature rotational relaxation of N<sub>2</sub> in collisions with Ne," *J. Phys. Chem. A* **105**, 6976 (2011).
- <sup>50</sup>H. Mori, T. Ishida, Y. Aoki, and T. Niimi, "Spectroscopic study of REMPI for rotational temperature measurement in highly rarefied gas," *AIP Conf. Proc.* **585**, 956 (2001).
- <sup>51</sup>B. O. Roos, K. Andersson, and M. P. Fulscher, "Towards an accurate molecular orbital theory for excited states: The benzene molecule," *Chem. Phys. Lett.* **192**, 5 (1992).
- <sup>52</sup>L. Streit, F. B. C. Machado, and R. Custodio, "Double ionization energies of HCl, HBr, Cl<sub>2</sub> and Br<sub>2</sub> molecules: An MRCI study," *Chem. Phys. Lett.* **506**, 22 (2011).
- <sup>53</sup>See <http://www.chem.uci.edu/~dmitryf/manuals/Fundamentals/Fluorescence%20Spectroscopy.pdf> for introduction to fluorescence Spectroscopy. PerkinElmer Inc.
- <sup>54</sup>B. Yuan and E. R. Bernstein, "Initial mechanisms for the unimolecular decomposition of electronically excited nitrogen-rich energetic materials with tetrazole rings: 1-DTE, 5—DTE, BTA, and BTH," *J. Chem. Phys.* **144**, 234302 (2016).
- <sup>55</sup>See supplementary material at <http://dx.doi.org/10.1063/1.4960345> for the comparison of a full CASSCF and different ONIOM approaches for (NH<sub>4</sub>)<sub>2</sub>BT.